Atmos. Chem. Phys., 26, 16857–16871, 2026
https://doi.org/10.5194/acp-26-16857-2026
© Author(s) 2026. This work is distributed under
the Creative Commons Attribution 4.0 License.

Atmospheric Chemistry and Physics
Open Access
EGU

Year-round aerosol variability across monsoon regimes at a near-equatorial Indian Ocean receptor

Krishnakant Babanrao Budhavant[1], Ahmed Muslim[2], Joakim Romson[3], Sreedharan Krishnakumari Satheesh[1], and Örjan Gustafsson[3]

[1]Divecha Centre for Climate Change, Indian Institute of Science, Bangalore 560012, India
[2]Maldives Meteorological Service, Gan, Addu City, 19070, Republic of Maldives
[3]Department of Environmental Science and the Bolin Centre for Climate Research, Stockholm University, Stockholm 10691, Sweden

Correspondence: Krishnakant Babanrao Budhavant (kbbudhavant@gmail.com) and Örjan Gustafsson (orjan.gustafsson@aces.su.se)

Received: 16 July 2026 – Discussion started: 20 August 2026
Revised: 2 October 2026 – Accepted: 5 November 2026 – Published: 25 November 2026

Abstract. Year-round observations of aerosol characteristics remain scarce over the equatorial Indian Ocean, particularly at receptor locations far from South Asian continental sources. Here, we present measurements of fine particulate matter ($PM_{2.5}$) chemical composition, aerosol optical properties, meteorology, air-mass transport, and five supporting dual-carbon isotope measurements from the Maldives Climate Observatory at Gan (MCOG; 0.69° S, 73.15° E) during the 2022 seasonal cycle.

During the northeast monsoon (NEM), continental influence from South and Southeast Asia coincided with higher $PM_{2.5}$ concentrations ($5.6 \pm 2.7\,\mu g\,m^{-3}$), aerosol optical depth at 500 nm (AOD_{500}; 0.17 ± 0.09), black carbon (BC), organic carbon (OC), and non-sea-salt sulfate. In the southwest monsoon (SWM), $PM_{2.5}$ and AOD_{500} were approximately 41 % and 35 % lower, respectively, while the relative contribution of marine aerosol increased. These differences likely reflect the combined influence of changes in air-mass origin and monsoon meteorology, including increased precipitation and wet scavenging during the SWM.

Despite pronounced changes in aerosol abundance and composition, the BC mass absorption cross-section at 658 nm ($BC\text{-}MAC_{658}$) differed only modestly between the NEM ($8.8 \pm 2.9\,m^2\,g^{-1}$) and SWM ($10.2 \pm 3.2\,m^2\,g^{-1}$), with no statistically significant seasonal difference. The isotope measurements showed substantial sample-to-sample variability, with fossil-dominated and mixed fossil–contemporary signatures occurring within both monsoon regimes.

These observations provide a year-round benchmark for aerosol transport, wet removal, composition, and BC absorption at a near-equatorial Indian Ocean receptor, complementary to previous measurements from the northern Maldives and useful for evaluating regional chemical-transport and Earth system models.

1 Introduction

Carbonaceous aerosols are among the most important atmospheric constituents influencing air quality, climate, and the global carbon cycle. Black carbon (BC) strongly absorbs solar radiation and contributes to atmospheric warming, whereas organic carbon (OC) exerts more complex radiative effects through both scattering and absorption depending on its composition and atmospheric evolution. Beyond their direct radiative impacts, carbonaceous aerosols modify cloud microphysics, influence precipitation processes, affect atmospheric chemistry, and contribute to regional climate variability (Bond et al., 2013; IPCC, 2021; Gustafsson et al., 2026).

The climatic effects of aerosols are particularly important over the Indian Ocean, where long-range transport of continental aerosols interacts with the seasonally reversing South Asian monsoon circulation. During the northeast mon-

soon (NEM), persistent northeasterly winds transport anthropogenic emissions, biomass-burning aerosols, and secondary pollutants from South and Southeast Asia across the Indian Ocean. In contrast, the southwest monsoon (SWM) introduces relatively clean marine air masses from the southern Indian Ocean, accompanied by increased precipitation, high relative humidity, and efficient wet scavenging. This seasonal reversal produces pronounced variations in aerosol loading, composition, and atmospheric processing, making the region a natural laboratory for investigating the evolution of carbonaceous aerosols during long-range transport (Ramanathan et al., 2001; Corrigan et al., 2006; Bosch et al., 2014; Budhavant et al., 2015, 2020).

Previous studies have established many important characteristics of South Asian aerosol outflow over the Maldives and northern Indian Ocean, including its seasonal transport, chemical composition, carbon sources, and optical properties (Novakov et al., 2000; Sheesley et al., 2012; Budhavant et al., 2015, 2018, 2024). However, substantially fewer year-round observations are available from the near-equatorial southern Indian Ocean receptor region. This limits our ability to assess how aerosol characteristics observed near South Asia persist or evolve during transport toward the equator, and how contrasting monsoon meteorology and removal processes influence the aerosol population reaching this region.

Atmospheric processing plays a critical role in determining the climatic impacts of carbonaceous aerosols. During long-range transport, BC particles undergo physical and chemical transformations through condensation of secondary inorganic and organic species, heterogeneous reactions, cloud processing, and interactions with water vapour. These processes can modify particle mixing state and morphology, enhancing light absorption and altering aerosol radiative forcing (Bond et al., 2013; Liu et al., 2017). Wet scavenging substantially reduces aerosol loading while simultaneously altering aerosol composition. However, continued atmospheric processing during marine transport can modify particle mixing and BC absorption efficiency (Budhavant et al., 2020, 2023). Consequently, aerosol optical properties cannot be inferred solely from BC mass concentrations; they also depend on atmospheric processing, particle mixing state, and transport history. Reliable identification of aerosol sources is equally important for understanding atmospheric evolution. Carbon isotope measurements provide valuable constraints on the relative contributions of fossil and contemporary carbon sources, complementing conventional chemical tracers and transport analyses. However, because radiocarbon analyses are analytically demanding and generally available only for selected samples, isotope observations are most powerful when interpreted alongside year-round measurements of aerosol chemistry, optical properties, and air-mass transport. Interpreted together, these measurements can help distinguish changes in aerosol abundance and composition from possible post-emission changes in optical properties and provide complementary constraints on source characteristics and atmospheric processing.

The Maldives Climate Observatory at Gan (MCOG) is located on the equatorial Indian Ocean, where the seasonally reversing monsoon circulation alternately transports polluted continental outflow from South and Southeast Asia during the NEM and predominantly marine air masses from the southern Indian Ocean during the SWM (Fig. 1). This geographical setting complements previous observations from the Maldives Climate Observatory at Hanimaadhoo (MCOH) in the northern Maldives, which is closer to the Indian subcontinent and particularly well positioned to characterise South Asian continental outflow. In contrast, MCOG (0.69° S), located at the southern end of the Maldives and close to the equator, is influenced by Northern Hemisphere continental outflow during the NEM and predominantly Southern Hemisphere marine air during the SWM. It therefore provides an opportunity to examine the persistence and transformation of South Asian aerosols farther from their continental sources and under contrasting equatorial marine conditions.

Year-round aerosol observations from this remote equatorial receptor are particularly valuable because transport pathways, precipitation, wet scavenging, relative humidity, and atmospheric processing can differ substantially from those affecting the northern Maldives. Such observations provide complementary constraints for evaluating the representation of aerosol transport and removal in regional chemical-transport and climate models. Aerosol–cloud–radiation interactions over the tropical Indian Ocean are also relevant to the broader South Asian monsoon system (Ramanathan et al., 2001; Li et al., 2016). Characterisation of the aerosol population reaching this near-equatorial marine environment therefore provides useful observational context for investigating these interactions. Direct evaluation of cloud responses, however, requires dedicated CCN and cloud-microphysical observations.

In this study, we present year-round observations of $PM_{2.5}$ chemical composition, aerosol optical properties, air-mass transport, and representative dual-carbon-isotope measurements collected at MCOG in 2022. To our knowledge, comparable year-round, co-located observations that combine these aerosol characteristics have not been reported from MCOG. Rather than treating the established NEM–SWM contrast itself as a new finding, we use these observations to quantify how the combined effects of monsoon circulation, air-mass origin, precipitation and atmospheric removal regulate aerosol loading and composition at this near-equatorial receptor. We further examine whether BC mass-normalised absorption varies between the contrasting transport regimes and use the available dual-carbon-isotope measurements as complementary evidence of carbon-source variability. The present observations are also evaluated in the context of earlier measurements in the Maldives and the Indian Ocean to

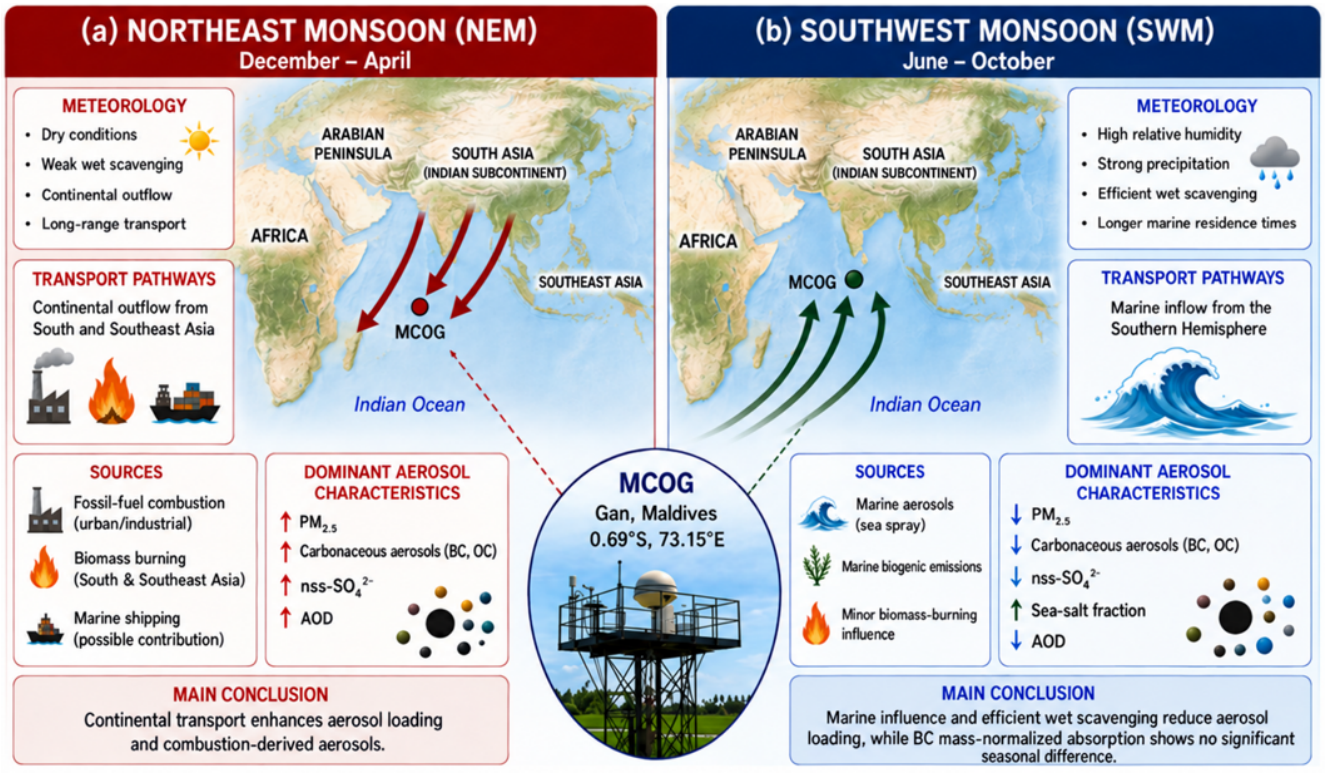


Figure 1. Conceptual framework illustrating the contrasting aerosol regimes associated with the northeast monsoon (NEM) and southwest monsoon (SWM) over the equatorial Indian Ocean. During the NEM, continental outflow from South and Southeast Asia transports combustion-derived aerosols, resulting in enhanced aerosol loading, carbonaceous aerosol concentrations, non-sea-salt sulfate, and aerosol optical depth. During the SWM, marine inflow from the southern Indian Ocean is characterised by higher relative humidity, increased precipitation, efficient wet scavenging, and a greater relative contribution of sea-salt aerosol. The Maldives Climate Observatory at Gan (MCOG) serves as a receptor site for investigating monsoon-driven variability in aerosol transport, chemical composition, atmospheric processing, optical properties, and source characteristics over the equatorial Indian Ocean.

assess the persistence or possible evolution of aerosol characteristics reaching the equatorial Indian Ocean.

Specifically, this study addresses the following questions:

1. How do contrasting monsoon transport pathways and meteorological conditions, including precipitation and wet removal, regulate aerosol loading and chemical composition at the near-equatorial MCOG receptor?

2. Does BC mass-normalised absorption vary systematically between the contrasting NEM and SWM aerosol regimes despite large seasonal changes in aerosol abundance and composition?

3. What complementary information do the available dual-carbon isotope measurements provide on carbon-source variability, and how do the contemporary MCOG observations compare with earlier measurements from the Maldives and Indian Ocean region?

By combining transport analysis, aerosol chemistry, optical properties, and supporting isotope observations, this study provides a year-round observational benchmark for carbonaceous aerosols at a near-equatorial Indian Ocean receptor. The measurements quantify the combined influence of monsoon transport and meteorological removal on aerosol loading and composition, evaluate whether BC mass-normalised absorption differs between contrasting monsoon regimes, and place contemporary MCOG observations in the context of earlier measurements from the Maldives and Indian Ocean. These observations provide complementary constraints for evaluating aerosol transport, removal, and composition in regional chemical-transport and Earth system models.

2 Methods

2.1 Site description and aerosol sampling

Atmospheric aerosol measurements were conducted at the MCOG (0.69° S, 73.15° E, 5 m above mean sea level), located on Gan Island in Addu Atoll, the southernmost atoll of the Maldives in the equatorial Indian Ocean (Fig. 2). $PM_{2.5}$ aerosol samples were collected from December 2021–

January 2023, providing year-round coverage of the 2022 seasonal cycle, using a high-volume aerosol sampler installed on the atmospheric sampling tower at MCOG. Sampling was conducted on a regular schedule to capture the full seasonal cycle, including both the NEM (December–April) and the SWM (June–October), as well as transitional periods. This sampling period enabled characterisation of the contrasting monsoon regimes and the intervening transition periods at this near-equatorial receptor.

Fine particulate matter ($PM_{2.5}$) was collected using a high-volume aerosol sampler (Digitel DH-77, Digitel Elektronik AG, Switzerland) equipped with a $PM_{2.5}$ size-selective inlet (impactor with silicone-greased plate) and operated at a nominal flow rate of $500 \pm 10\,L\,min^{-1}$. Sampling and filter-handling procedures followed established approaches previously applied for $PM_{2.5}$ collection at Maldives receptor observatories using the same high-volume sampling system (Budhavant et al., 2018, 2024). Aerosol particles were collected on binder-free quartz filters (Millipore AQFA8X105, Merck, Ireland) cut to 150 mm diameter, which were pre-combusted by heating at 450 °C for 6 h before sampling, to remove residual organic contaminants. The filters were kept in pre-combusted, folded aluminum foil envelopes and then sealed in polyethylene bags. Before and after sampling, filters were weighed in a climate-controlled room (20 °C, 50 % RH) after at least 24 h of equilibration. Samples were stored at −20 °C except during transport and analysis. These procedures are consistent with earlier quality-controlled filter sampling approaches used for carbonaceous aerosol measurements in the Maldives (Budhavant et al., 2015, 2018).

Aerosol sampling was conducted using variable-duration filter collection periods, typically 72 h during the northeast monsoon and longer during other seasons when aerosol concentrations were lower. Sampling durations were adjusted to obtain sufficient particulate loading for subsequent analyses and to accommodate operational constraints, including nearby aircraft activities and station maintenance. Each filter therefore represents an integrated measurement over its respective sampling period. Consequently, the measurements are interpreted primarily at seasonal and monsoon-regime scales rather than as indicators of individual short-term events.

Instrument flow rates were calibrated regularly using a certified flow calibration system. Field blank filters were collected at regular intervals, handled identically to exposed samples except for active air sampling, and used to evaluate potential contamination during filter handling, transport, and laboratory processing.

2.2 Carbonaceous aerosols and chemical composition

Carbonaceous aerosol components, including OC and elemental carbon (EC), with EC used here as an operational proxy for black carbon (BC), were quantified using a thermal–optical carbon analyser (Model 4 L, Sunset Laboratory Inc., USA) following the NIOSH 5040 protocol. During analysis, filter punches ($1.5\,cm^2$) were subjected to a stepwise temperature program under helium and helium–oxygen atmospheres. Desorbed carbon during the helium phase was oxidised to CO_2 in an MnO_2 oven, and the remaining carbon was directly combusted during the helium-oxygen phase before passing through the MnO_2 oven. CO_2 was quantified with a flame ionisation detector (FID) after conversion to CH_4 in a methanator. At the end of every run, the FID response was calibrated using a pulse of 5 % CH_4 in He. Continuous laser transmittance (658 nm) measurements were used to correct for pyrolytic carbon formation and to determine the OC–BC split point. Instrument calibration was performed using NIST-traceable sucrose standards (SRM 8785), and routine quality control included calibration verification, replicate analyses, and blank corrections. Based on repeated analyses and calibration performance, the analytical uncertainties were estimated to be approximately ±10 % for OC and ±15 % for BC. Further details are provided in Budhavant et al. (2015, 2023).

Major water-soluble inorganic ions, Na^+, K^+, Ca^{2+}, Mg^{2+}, NH_4^+, Cl^-, Br^-, NO_3^-, and SO_4^{2-}, were measured by ion chromatography (Dionex Aquion system, Thermo Fisher Scientific, USA). Filter punches were extracted in Milli-Q water (18.2 MΩ cm, 0.22 µm filter) in 15 mL polypropylene centrifuge tubes and sonicated for 30 min prior to analysis. Anions were separated on an AS9-HC column, and cations on a CS12A column. Analytical precision for ion concentrations was typically better than 5 %; detection limits were $< 0.1\,\mu g\,m^{-3}$. More details are provided in Budhavant et al. (2023). To distinguish marine and non-marine contributions, concentrations of non-sea-salt sulfate (nss-SO_4^{2-}), nss-K^+, nss-Ca^{2+}, nss-Mg^{2+} and nss-Br^- were calculated using sodium (Na^+) as a conservative tracer of sea salt and the corresponding seawater ionic ratios following Keene et al. (1986).

$$\text{nss-}X = X_{\text{measured}} - \text{Na}^+ \times (X/\text{Na}^+)_{\text{seawater}}$$

where X denotes SO_4^{2-}, K^+, Ca^{2+}, Mg^{2+} and Br^-. Organic matter (OM) concentrations were derived from measured OC for the purpose of aerosol mass closure using an OM/OC conversion factor of 1.8, consistent with previous observations of aged continental aerosols transported over the Indian Ocean and South Asian outflow regions (Turpin and Lim, 2001; Budhavant et al., 2015, 2018). The selected conversion factor falls within the range commonly reported for moderately to highly oxidized atmospheric organic aerosols. It provides a reasonable estimate of particulate organic matter for regional mass closure. Because OM was not measured directly, these values are interpreted as estimated contributions rather than independently measured aerosol components.

Analytical uncertainties associated with carbonaceous species, inorganic ions, and derived parameters were considered in subsequent calculations and interpretation. Seasonal contrasts were evaluated using the statistical tests described

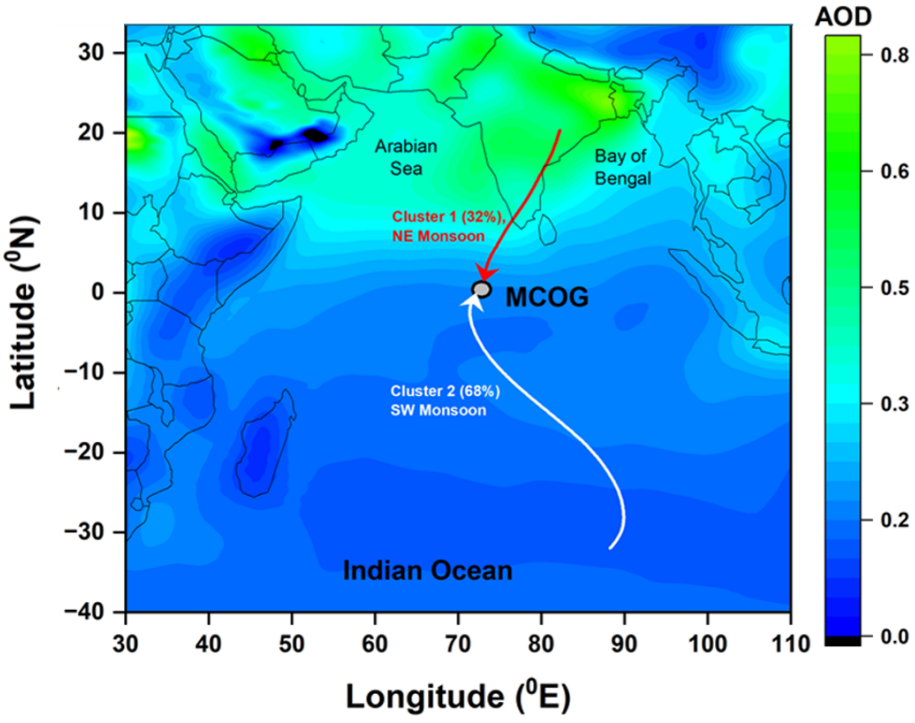


Figure 2. Dominant seasonal transport pathways to the Maldives Climate Observatory at Gan (MCOG), inferred from 10 d HYSPLIT backwards-trajectory clusters overlaid on the 2022 MODIS annual aerosol optical depth (AOD) distribution. Continental outflow during the northeast monsoon (red) originates from South and Southeast Asia, whereas predominantly marine air masses during the southwest monsoon (blue) originate over the southern Indian Ocean. Additional details regarding the trajectory clustering are provided in the Supplemental Information (Fig. S3).

below, and differences are interpreted in terms of both their statistical significance and magnitude, rather than by analytical uncertainty alone.

2.3 Aerosol optical properties

The optical properties of carbonaceous aerosols were characterised using the BC mass absorption cross-section (BC-MAC_{658}) and column-integrated aerosol optical depth (AOD). These complementary measurements provide information on the mass-normalised absorption of BC-containing aerosol collected at the surface and the total atmospheric aerosol loading, respectively.

The BC-MAC_{658} was estimated from filter-based optical attenuation measurements obtained using the Sunset Laboratory thermal–optical carbon analyser. Optical attenuation at the instrument laser wavelength (658 nm) was measured continuously during thermal analysis and combined with thermally determined BC mass concentrations to estimate BC-MAC_{658} following approaches previously applied over the Indian Ocean (Ram and Sarin, 2009; Budhavant et al., 2020, 2024; Nair et al., 2024). The aerosol absorption coefficient was derived from the measured optical attenuation using a multiple-scattering correction factor of 4.5 (Weingartner et al., 2003; Budhavant et al., 2024). BC-MAC_{658} was calculated as the ratio of the aerosol absorption coefficient to the corresponding BC mass concentration. BC-MAC_{658} represents the mass-normalised light absorption of BC-containing aerosol and may be influenced by several factors, including particle mixing state, secondary coatings, source characteristics, morphology, and atmospheric processing. Accordingly, variations in BC-MAC_{658} are not interpreted as a direct or unique measure of atmospheric ageing. It should be noted that BC-MAC_{658} provides no direct measurement of particle morphology or internal mixing state.

Column-integrated AOD was obtained from a CIMEL sun–sky radiometer operated as part of the Aerosol Robotic Network (AERONET) at MCOG. Only Version 3 Level 2.0 quality-assured data, representing 230 measurement days, were used in this study. The AERONET processing algorithm includes automatic cloud screening, instrument calibration, and standardised quality-control procedures, ensuring high-quality and globally consistent aerosol optical measurements (Holben et al., 1998; Giles et al., 2019). Daily mean AOD at 500 nm (AOD_{500}) was used to characterise seasonal changes in column aerosol loading and to complement the surface-based $PM_{2.5}$observations.

2.4 Meteorological measurements and air-mass trajectory analysis

Meteorological parameters, including air temperature, relative humidity (RH), precipitation, wind speed, and wind direction, were obtained from the Maldives Meteorological Service station located adjacent to the MCOG. These observations were used to characterize seasonal meteorological conditions and to interpret variations in aerosol loading, chemical composition, optical properties, and atmospheric processing associated with the monsoon circulation. In particular, precipitation and RH were considered when evaluating the potential influence of wet scavenging and humid marine conditions on aerosol concentrations. Thus, seasonal aerosol variability was interpreted in the combined context of air-mass origin and local/regional meteorological conditions rather than being attributed solely to transport pathways.

Air-mass transport pathways were investigated using the Hybrid Single-Particle Lagrangian Integrated Trajectory (HYSPLIT, version 5.4.2) model developed by the NOAA Air Resources Laboratory (Draxler and Hess, 1998; Stein et al., 2015). Ten-day backward trajectories were calculated four times daily (00:00, 06:00, 12:00, and 18:00 UTC) using an arrival height of 50 m above ground level, consistent with previous trajectory analyses at the MCOG that focused on near-surface marine air masses (e.g., Budhavant et al., 2024). Meteorological input fields were obtained from the Global Data Assimilation System (GDAS) with a horizontal resolution of $1^\circ \times 1^\circ$. The 10 d trajectory length was selected to capture long-range transport from major continental and marine source regions.

Trajectory clustering was performed using the Total Spatial Variance (TSV) method implemented within HYSPLIT to identify the dominant transport regimes and reduce trajectory complexity. Two major trajectory clusters were identified, representing continental and marine transport pathways (Fig. S3), and were subsequently used, together with observed meteorological conditions, to interpret seasonal variations in aerosol loading, chemical composition, optical properties, and isotope signatures. The trajectory clusters are used here to characterise the dominant transport history and probable source-region influence and are not interpreted as quantitative source apportionment. Although uncertainties in individual trajectories increase with transport time, the ensemble trajectory analysis provides a useful representation of the dominant seasonal transport patterns influencing MCOG. The interpretation therefore considers the consistency among trajectory clusters, observed winds, precipitation, RH, and aerosol measurements rather than relying on individual trajectories alone.

2.5 Dual-carbon isotope measurements and analysis

A subset of $PM_{2.5}$ samples was selected for dual-carbon isotope analysis. Five samples representing the NEM and SWM periods were analysed. The selected samples had relatively high BC concentrations to ensure sufficient carbon mass for accurate radiocarbon ($\Delta^{14}C$) and stable carbon isotope ($\delta^{13}C$) measurements. Because sample selection was constrained by carbon-mass requirements, the isotope subset was not intended to represent the full seasonal distribution of BC sources. Rather, the measurements provide complementary source information for selected periods within the year-round dataset.

BC was isolated from quartz fiber filters using the thermal–optical transmission method described previously, coupled with online CO_2 collection following established procedures (Zencak et al., 2007; Chen et al., 2013; Andersson et al., 2015; Budhavant et al., 2015, 2023). During thermal–optical analysis, the BC fraction was evolved under controlled heating conditions, and the resulting CO_2 was purified using magnesium perchlorate and silver wool traps to remove water vapor and halogen-containing gases, respectively. The purified CO_2 was cryogenically trapped in liquid nitrogen and flame-sealed in pre-combusted borosilicate glass ampoules for isotope analysis.

Radiocarbon ($\Delta^{14}C$) and stable carbon isotope ($\delta^{13}C$) measurements were performed at the Department of Physics and Astronomy, Uppsala University, Sweden. Radiocarbon signatures were used to distinguish fossil-fuel-derived BC ($\Delta^{14}C \approx -1000‰$) from contemporary biomass-derived carbon, while $\delta^{13}C$ provided complementary information on carbon source characteristics (Gustafsson et al., 2009; Bosch et al., 2014; Kirillova et al., 2013, 2014; Andersson et al., 2015; Budhavant et al., 2023). The relative fossil and contemporary biomass-derived contributions reported in Table S2 in the Supplement were estimated using a two-endmember $\Delta^{14}C$ mass-balance approach following the methodology applied in previous South Asian and Indian Ocean studies (Dasari et al., 2020; Budhavant et al., 2023). The resulting fractions are used as sample-specific source constraints rather than as seasonal mean source contributions. The combined $\Delta^{14}C$ and $\delta^{13}C$ measurements were therefore used as qualitative, source-diagnostic constraints alongside aerosol chemistry and transport information. Given the limited, selectively sampled dataset, the isotope measurements were not used for quantitative seasonal source apportionment or for statistical comparison between the NEM and SWM.

Seasonal differences between the NEM and SWM were evaluated using Welch's t-test and Mann–Whitney U-test. Statistical significance was defined as $p < 0.05$. Because statistical significance does not necessarily indicate a large or physically important difference, seasonal contrasts were interpreted by considering the magnitude and variability of the observations together with the statistical tests. The limited dual-carbon isotope dataset was not subjected to seasonal statistical testing.

3 Results and discussion

3.1 Monsoon meteorology, transport pathways, and aerosol loading

The meteorological observations during 2022 were consistent with the established seasonal reversal of the South Asian monsoon described in previous studies (Figs. S1 and S2 in the Supplement). During the NEM, relatively dry conditions and persistent northeasterly winds prevailed, whereas the SWM was characterised by southwesterly winds, higher relative humidity, and substantially more frequent and intense precipitation. These contrasting conditions are important not only for air-mass transport but also for aerosol removal, particularly through enhanced wet scavenging during the SWM.

The contrasting meteorological regimes were consistent with the HYSPLIT backward trajectories (Fig. 2). During the NEM, air masses predominantly originated over South and Southeast Asia before reaching MCOG, whereas during the SWM trajectories remained largely confined to the southern Indian Ocean, indicating a predominantly marine influence. Trajectory cluster analysis further showed that continental transport accounted for approximately 32 % of all air masses arriving at MCOG, while marine transport represented the remaining 68 % (Fig. S3). Continental trajectories crossed densely populated and industrialized regions where anthropogenic emissions, biomass burning, and secondary aerosol formation are major aerosol sources, whereas marine trajectories originated over the remote southern Indian Ocean and were associated with comparatively clean oceanic air masses.

The MODIS annual AOD distribution provides additional regional context for these transport pathways (Fig. 2), showing higher aerosol loading over South Asia and the northern Indian Ocean and substantially lower aerosol loading over the remote southern Indian Ocean. Together, the trajectory analysis and meteorological observations identify two contrasting monsoon regimes that influence MCOG: a continental influence during the NEM and a predominantly marine influence during the SWM.

These contrasting transport and meteorological regimes coincided with clear differences in the observed aerosol loading. $PM_{2.5}$ concentrations exhibited a pronounced seasonal cycle, averaging $5.6 \pm 2.7\,\mu g\,m^{-3}$ during the NEM and decreasing to $3.3 \pm 1.3\,\mu g\,m^{-3}$ during the SWM, corresponding to an approximately 41 % lower seasonal mean during the SWM; the difference was statistically significant ($p < 0.001$; Table 1, Fig. 3). A similar seasonal pattern was observed for AOD_{500}, which decreased from 0.17 ± 0.09 during the NEM to 0.11 ± 0.04 during the SWM (approximately 35 % lower; $p < 0.001$; Table 1, Fig. 5).

The consistent seasonal behaviour of surface $PM_{2.5}$, column-integrated AOD, together with the trajectory and meteorological observations, indicates that aerosol loading at MCOG reflects the combined effects of changing air-mass origin and monsoon meteorology. Cleaner marine inflow dur-

Table 1. Summary of aerosol properties measured at the Maldives Climate Observatory-Gan during December 2021–January 2023. Reported parameters include sampling period, aerosol optical depth (AOD), number of samples, $PM_{2.5}$ mass concentration and mass absorption cross-sections of black carbon at 658 nm (BC–MAC_{658}), BC, organic carbon (OC), and major inorganic ions.

Sampling period	AOD	No. of samples	$PM_{2.5}$ ($\mu g\,m^{-3}$)	BC-MAC_{658} ($m^2\,g^{-1}$)	BC ($\mu g\,m^{-3}$)	OC ($\mu g\,m^{-3}$)	nss-SO_4^{2-} ($\mu g\,m^{-3}$)	NO_3^- ($ng\,m^{-3}$)	nss-K^+ ($ng\,m^{-3}$)	nss-Ca^{2+} ($ng\,m^{-3}$)	nss-Br^- ($ng\,m^{-3}$)
NE monsoon	0.17 ± 0.09	46	5.59 ± 2.7	8.81 ± 2.87	0.21 ± 0.18	0.65 ± 0.70	1.32 ± 0.7	24 ± 9	90 ± 63	47 ± 43	28 ± 17
Pre-transition	0.10 ± 0.04	8	2.79 ± 1.0	9.53 ± 2.31	0.04 ± 0.03	0.18 ± 0.13	0.52 ± 0.3	18 ± 4	25 ± 15	51 ± 46	42 ± 14
SW Monsoon	0.11 ± 0.04	26	3.29 ± 1.3	10.2 ± 3.18	0.05 ± 0.05	0.23 ± 0.19	0.50 ± 0.4	24 ± 10	27 ± 34	27 ± 33	41 ± 25
Post-transition	0.11 ± 0.04	7	2.65 ± 1.4	8.65 ± 2.54	0.05 ± 0.02	0.17 ± 0.03	0.44 ± 0.3	21 ± 4	19 ± 12	13 ± 9	48 ± 17
Annual	0.14 ± 0.08	87	4.41 ± 2.5	9.28 ± 2.90	0.14 ± 0.15	0.44 ± 0.46	0.93 ± 0.7	23 ± 9	60 ± 59	39 ± 39	35 ± 19

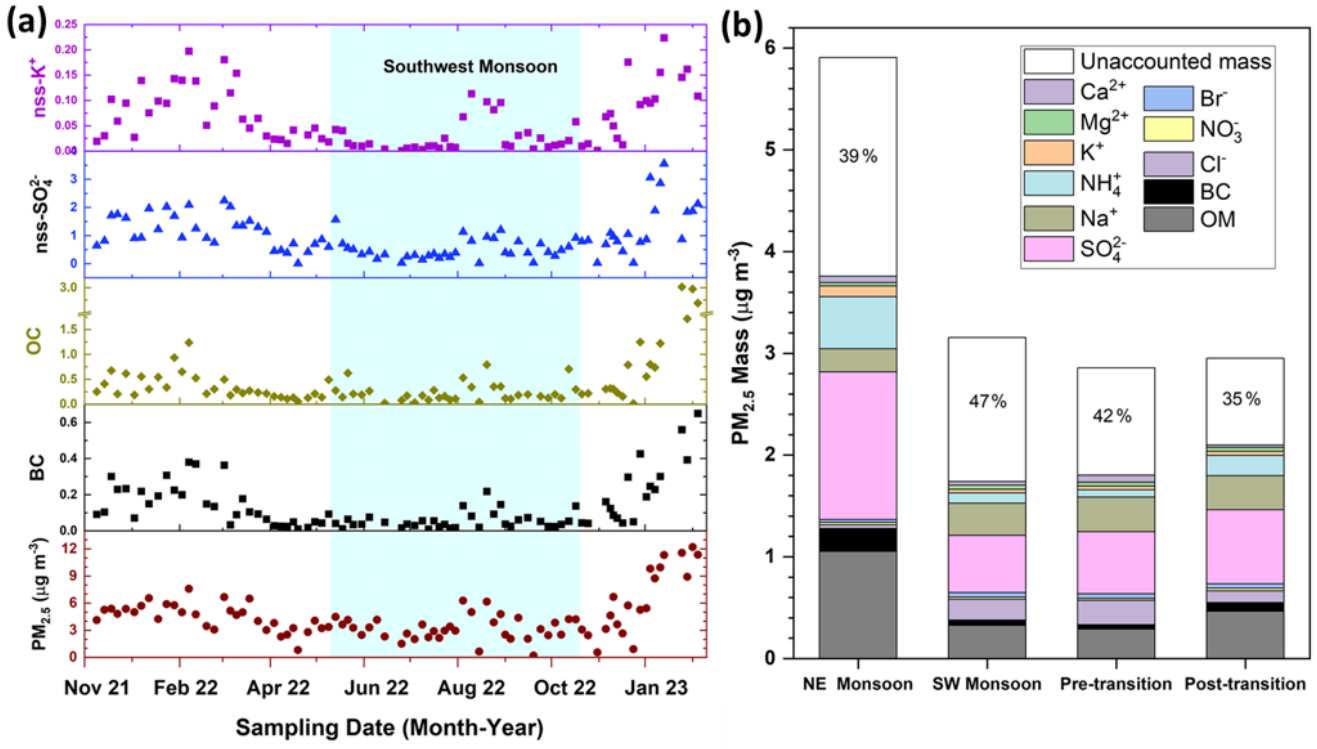


Figure 3. Panel **(a)** Time series of $PM_{2.5}$ mass concentration and major aerosol chemical components measured at the Maldives Climate Observatory at Gan (MCOG) during 2022, including elemental carbon (BC), organic matter (OM), non-sea-salt sulfate (nss-SO_4^{2-}), and non-sea-salt potassium (nss-K^+). The cyan-shaded region denotes the southwest monsoon (SWM). **(b)** Mean chemical composition of $PM_{2.5}$ during the northeast monsoon (NEM), pre-transition, SWM, and post-transition periods, showing the relative contributions of water-soluble inorganic ions, carbonaceous components (OM and BC), and the unidentified residual fraction.

ing the SWM likely contributes to the lower aerosol burden, while the substantially greater precipitation provides an additional removal mechanism through wet scavenging. The present observations do not permit these two influences to be quantitatively separated.

Measurable $PM_{2.5}$ levels persisted during the SWM despite the predominantly marine influence, indicating a persistent regional background aerosol burden. Because the $PM_{2.5}$ samples represent 72 h integrations, these differences are interpreted at the seasonal and monsoon-regime scale rather than as responses to individual rainfall or transport events.

3.2 Monsoon-driven changes in aerosol chemistry and source signatures

3.2.1 Seasonal variability in aerosol chemical composition

The pronounced seasonal differences in aerosol loading were accompanied by clear changes in aerosol chemical composition, reflecting the alternating influence of continental outflow and marine inflow associated with the South Asian monsoon (Fig. 3; Table 1). Carbonaceous aerosol components and secondary inorganic species were substantially enhanced during the NEM, whereas marine-derived constituents became relatively more important during the SWM. The pre- and post-monsoon transition periods exhibited intermediate chemical characteristics, reflecting the progressive replacement of continental air masses by marine inflow during monsoon onset and the gradual re-establishment of continental influence during monsoon withdrawal.

Concentrations of BC, OC, OM, and nss-SO_4^{2-} were all statistically higher during the NEM than during the SWM ($p < 0.001$; Table 1). The transition periods generally showed intermediate concentrations, consistent with the gradual evolution of air-mass origin and changes in weather, rather than abrupt changes in aerosol composition. Elevated concentrations of carbonaceous aerosols and nss-SO_4^{2-} during the NEM are consistent with efficient long-range transport of combustion-derived aerosols and secondary sulfate from South and Southeast Asia. However, the lower concentrations observed during the SWM likely reflect both the reduced influence of continental emissions and more efficient aerosol removal under wetter monsoon conditions. Thus, the seasonal concentration differences cannot be attributed to source-region changes alone.

These observations agree with previous studies over the northern Indian Ocean and South Asian outflow, which have demonstrated enhanced transport of anthropogenic aerosols during the winter monsoon (Ramanathan et al., 2001; Stone et al., 2007; Budhavant et al., 2020, 2023; Clarke et al., 2026).

Although the absolute concentrations of sea-salt ions also varied seasonally, the relative contributions of Na^+ and Cl^- to $PM_{2.5}$ increased during the SWM ($p < 0.05$), indicating a transition from a pollution-dominated aerosol regime during the NEM to a more marine-influenced aerosol composition. This change in relative composition occurred while total $PM_{2.5}$ was lower, consistent with the combined effects of stronger marine influence and enhanced removal of continental aerosol. The transition periods bridged these contrasting seasonal regimes, with continental tracers progressively decreasing at monsoon onset and increasing at monsoon withdrawal, reflecting the seasonal evolution of transport pathways.

3.2.2 Diagnostic aerosol ratios and seasonal changes in source influence

Diagnostic aerosol ratios provide additional insight into seasonal variations in aerosol sources and chemical processing beyond what concentration measurements alone can provide (Fig. 4). Seasonal correlation patterns among major aerosol species further support these changes in aerosol composition and source characteristics (Fig. S4 in the Supplement).

The OC/BC ratio was significantly higher during the SWM than during the NEM (4.89 ± 2.67 vs. 3.22 ± 1.97, Mann–Whitney $p < 0.001$; Fig. 4e), indicating a greater relative contribution of organic carbon under marine conditions. Lower OC/BC ratios during the NEM are consistent with a stronger relative influence of combustion-derived continental aerosol, whereas higher SWM values may also reflect differential removal and atmospheric processing during marine transport (Bosch et al., 2014; Budhavant et al., 2015, 2020). Because OC/BC can be influenced by both source mixtures and atmospheric processing, it is treated here as a diagnostic indicator rather than a unique source tracer. The transition periods exhibited intermediate values, reflecting the gradual shift between continental and marine air masses and weather conditions.

The NH_4^+/nss-SO_4^{2-} ratio also differed significantly between the two monsoon seasons ($p < 0.001$; Fig. 4a), with higher and more variable values during the SWM. The nss-SO_4^{2-}/NO_3^- ratio was higher during the NEM ($p < 0.001$; Fig. 4b), indicating a stronger relative contribution of sulfate than nitrate during continental influence. These ratios may reflect differences in precursor sources, secondary aerosol formation, transport history, and differential removal, and therefore should not be interpreted solely in terms of source-region changes.

The Cl^-/Na^+ ratio increased significantly during the SWM ($p < 0.001$; Fig. 4c), consistent with a stronger contribution of fresh marine sea salt. Because chloride can also be modified by atmospheric processing, the seasonal change is interpreted primarily as evidence of increased marine influence rather than as a quantitative indicator of sea-salt age. The nss-K^+/BC ratio showed considerable temporal variability but no significant seasonal difference (Fig. 4d). Consequently, this ratio is interpreted only as a qualitative indicator of source variability because non-sea-salt potassium also has non-combustion sources (Safai et al., 2010). No seasonal change in biomass-burning contribution is inferred from this ratio alone.

Overall, the diagnostic ratios demonstrate systematic seasonal changes in aerosol composition that are consistent with varying continental and marine influence and atmospheric processing, while the transition periods exhibited intermediate characteristics consistent with the gradual evolution of monsoon circulation. Together with the transport analysis, meteorological measurements, and concentration measurements presented in Sects. 3.1 and 3.2.1, these ratios provide complementary evidence that the aerosol population reaching MCOG varies between the contrasting monsoon regimes. However, the ratios alone do not provide quantitative source apportionment.

3.3 Seasonal variability in BC optical properties over the equatorial Indian Ocean

3.3.1 Seasonal variability in BC-MAC and aerosol optical depth

Aerosol optical properties exhibited contrasting responses to seasonal monsoon circulation (Fig. 5; Table 1). As discussed in Sect. 3.1, AOD_{500} followed the seasonal behaviour of $PM_{2.5}$, with lower values during the SWM (Fig. 5), consistent with the lower aerosol burden under the combined influence of predominantly marine inflow and enhanced wet removal.

In contrast, BC-MAC_{658} exhibited only modest seasonal variability. Mean BC-MAC_{658} increased from $8.8 \pm 2.9\,m^2\,g^{-1}$ during the NEM to $10.2 \pm 3.2\,m^2\,g^{-1}$ during the SWM; however, this difference was not statistically significant (Welch's t-test, $p = 0.103$; Mann–Whitney U-test, $p = 0.064$; Table S1 in the Supplement). The substantial overlap between the seasonal distributions indicates that the average light-absorbing efficiency of BC remained broadly comparable under the contrasting monsoon regimes.

Thus, while aerosol loading and chemical composition changed markedly between the NEM and SWM, BC mass-normalised absorption remained comparatively stable. The slightly higher mean BC-MAC_{658} during the SWM is therefore treated as a tendency rather than evidence of a systematic seasonal enhancement in BC absorption.

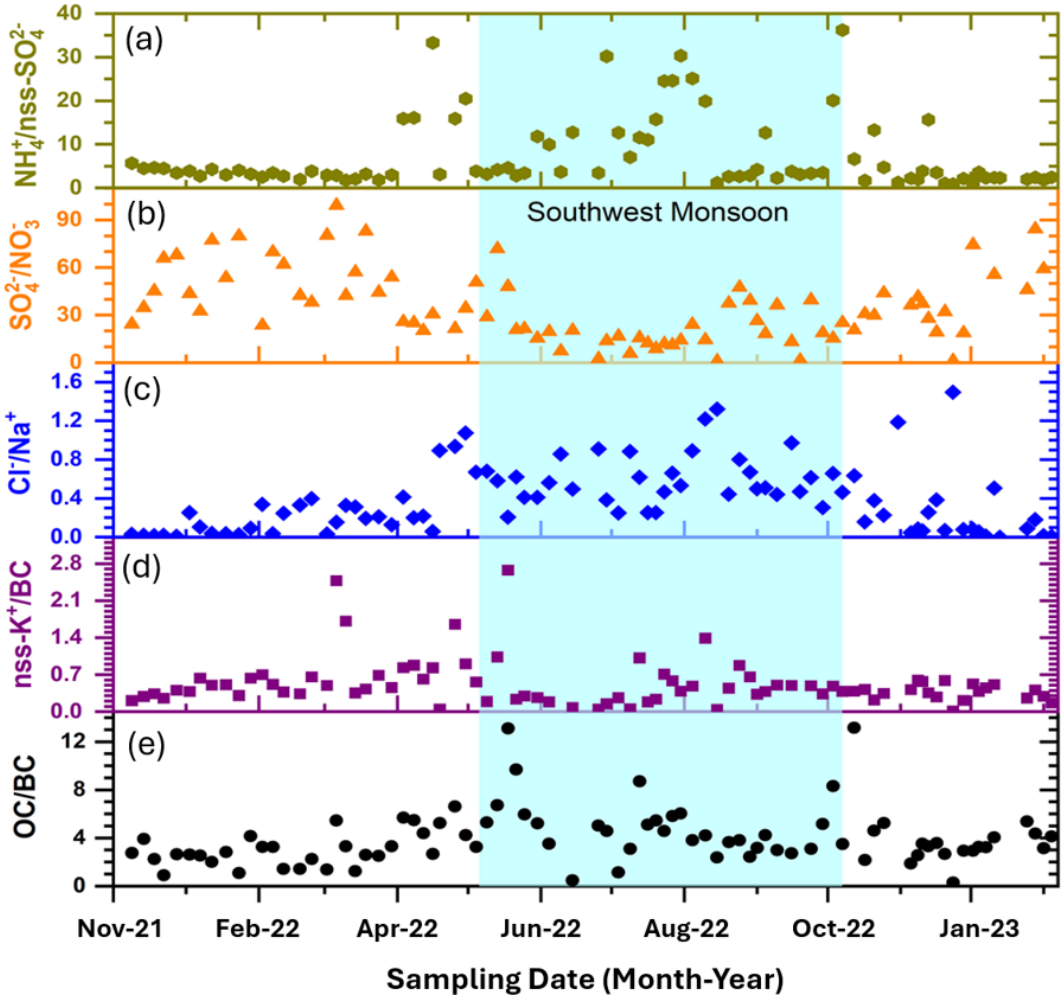


Figure 4. Seasonal variability of aerosol diagnostic ratios measured at the Maldives Climate Observatory at Gan (MCOG) during December 2021–January 2023: **(a)** NH_4^+/nss-SO_4^{2-}, **(b)** nss-SO_4^{2-}/NO_3^-, **(c)** Cl^-/Na^+, **(d)** nss-K^+/BC, and **(e)** OC/BC. Shaded regions denote the northeast monsoon (NEM), southwest monsoon (SWM), and the intervening transition periods. The seasonal evolution of these diagnostic ratios illustrates changes in the relative influence of continental and marine aerosol sources, secondary aerosol composition, and aerosol source characteristics associated with monsoon-driven transport over the equatorial Indian Ocean.

3.3.2 Atmospheric processing and interpretation for BC optical properties

The seasonal evolution of BC optical properties is interpreted in the context of the contrasting meteorological conditions, transport pathways, and aerosol chemistry over the equatorial Indian Ocean. During the SWM, persistently high relative humidity, frequent precipitation, and predominantly marine air masses provide favourable conditions for aqueous-phase oxidation and secondary aerosol formation during long-range transport (Bond et al., 2013; Liu et al., 2017). At the same time, frequent precipitation efficiently removes aerosol particles through wet scavenging and may alter the composition of the aerosol population remaining in the atmosphere.

The aerosol chemical observations are broadly consistent with this interpretation. Sulfate remained the dominant secondary inorganic aerosol throughout the year, while the significantly higher OC/BC ratios observed during the SWM indicate a greater relative contribution of organic aerosol under marine conditions. In addition, the significantly higher Cl^-/Na^+ ratio during the SWM ($p < 0.001$) reflects the increased influence of relatively fresh marine sea salt. However, these chemical indicators can be affected by changes in sources, atmospheric processing, and differential removal, and therefore do not provide direct evidence of changes in BC coating thickness, morphology, or internal mixing state.

The HYSPLIT trajectory analysis further shows that SWM air masses travelled predominantly over the southern Indian Ocean before reaching MCOG. Such marine transport provides opportunities for atmospheric processing, but the BC-

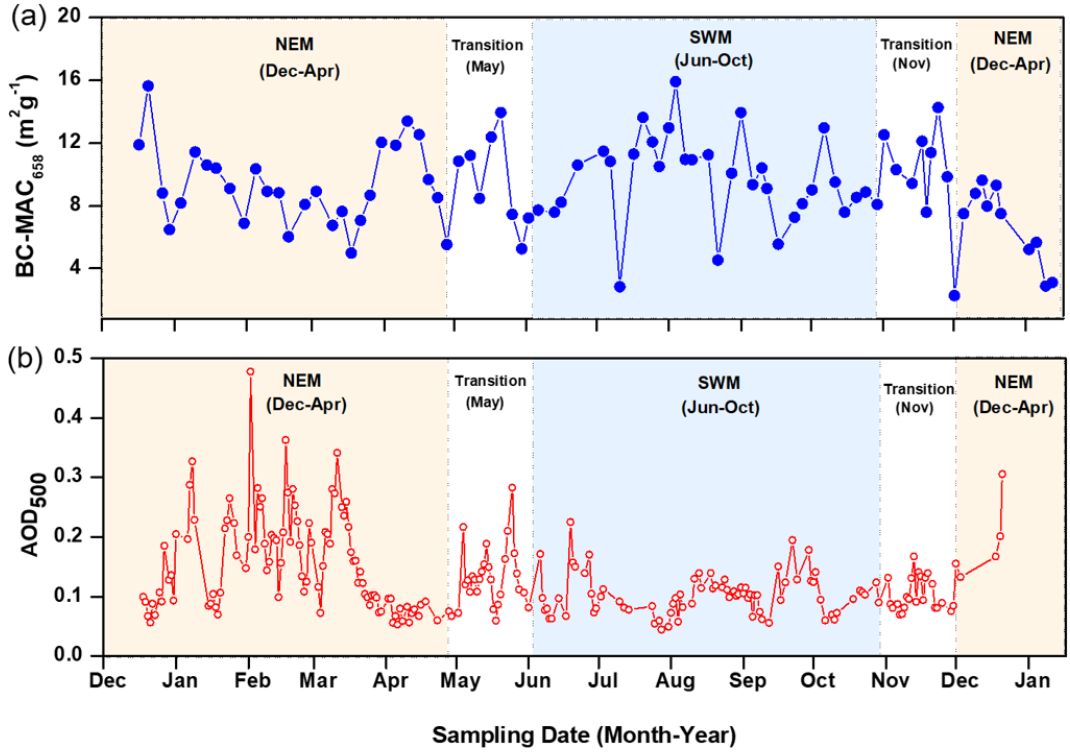


Figure 5. Seasonal variability of **(a)** black carbon mass absorption cross-section at 658 nm (BC-MAC_{658}) and **(b)** aerosol optical depth at 500 nm (AOD_{500}) measured at the Maldives Climate Observatory at Gan (MCOG) from December 2021–January 2023. Shaded regions denote the northeast monsoon (NEM), southwest monsoon (SWM), and the intervening transition periods. AOD_{500} exhibits a pronounced seasonal cycle, with higher values during the NEM, which correspond to enhanced continental aerosol loading. In contrast, BC-MAC_{658} shows only modest seasonal variability despite the substantial changes in aerosol loading between the two monsoon regimes.

MAC_{658} observations do not show a statistically significant seasonal response. Consequently, the present dataset cannot attribute the slightly higher mean SWM BC-MAC_{658} specifically to atmospheric ageing or enhanced BC coatings. Alternative influences, including differences in source mixtures, wet removal, aerosol composition, and the selective persistence of particles during transport, cannot be separated with the available measurements.

The observed BC-MAC_{658} values nevertheless fall within the range previously reported for aged aerosols over the northern Indian Ocean and South Asian outflow regions (Budhavant et al., 2020, 2024). This consistency suggests that despite large seasonal differences in BC abundance and aerosol composition, mass-normalised BC absorption at MCOG remains within the range previously observed during long-range transport over the Indian Ocean.

Overall, the observations demonstrate a stronger seasonal response in aerosol abundance and composition than in BC-MAC_{658}. Direct characterisation of BC mixing state, coating thickness, and particle morphology would be required to determine whether atmospheric processing causes systematic changes in BC absorption during transport to MCOG.

3.4 Supporting dual-carbon isotope evidence for aerosol source variability

Dual-carbon isotope measurements were performed on five $PM_{2.5}$ samples to provide an independent assessment of carbon source characteristics over the equatorial Indian Ocean (Fig. 6). Owing to the analytical complexity and high carbon mass requirements of radiocarbon analysis, isotope measurements were restricted to samples with sufficiently high carbon loading. Consequently, the isotope dataset represents a targeted subset of the year-round observations and is interpreted as complementary evidence rather than a comprehensive seasonal source-apportionment dataset.

The isotope signatures span a broad range among the five analysed samples (Fig. 6; Table S2). During the NEM, the February sample was strongly fossil-dominated ($f_{fossil} = 0.99$), whereas the March sample showed a substantially larger contemporary biomass-derived contribution ($f_{biomass} = 0.64$). The January 2023 sample showed an intermediate source composition, with fossil and biomass-derived fractions of 0.61 and 0.39, respectively. A similarly large contrast occurred during the SWM: the July sample was strongly fossil-dominated ($f_{fossil} = 0.99$), whereas the September sample showed a substantially larger contempo-

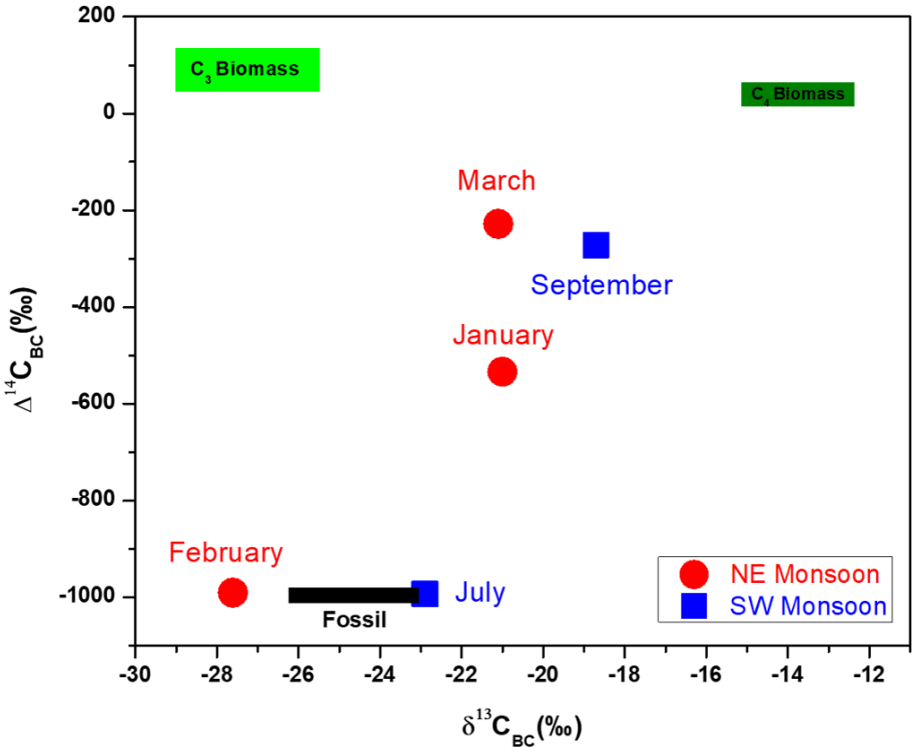


Figure 6. Dual-carbon isotope signatures ($\delta^{13}C$ and $\Delta^{14}C$) of black carbon (BC) measured at the Maldives Climate Observatory at Gan (MCOG). Circles and squares represent samples collected during the northeast monsoon (NEM) and southwest monsoon (SWM), respectively. Shaded boxes indicate the approximate isotopic ranges of fossil-fuel, C_3 biomass, and C_4 biomass endmembers based on previous studies (Budhavant et al., 2023). The broad range of isotope signatures within both monsoon periods illustrates substantial sample-to-sample source heterogeneity; given the limited number of measurements, the data are not interpreted as quantitative seasonal source apportionment.

rary biomass-derived contribution ($f_{\text{biomass}} = 0.61$). Thus, fossil-dominated and mixed fossil–contemporary signatures occurred in both monsoon regimes, indicating substantial source heterogeneity among samples rather than a clear NEM–SWM separation.

The accompanying $\delta^{13}C$ variability provides additional information on differences in carbon-source characteristics. However, because only five selectively sampled filters were analysed, the isotope dataset does not support quantitative seasonal source apportionment or statistical comparison between the monsoon periods. The isotope results therefore do not establish a distinct seasonal source regime; instead, they provide independent evidence of substantial source heterogeneity within both monsoon conditions and a complementary context for the variability inferred from aerosol chemistry and transport observations.

3.5 Context of the present observations within earlier Maldives measurements

Earlier observations across the Maldives provide useful quantitative context for the present MCOG dataset, although they should not be interpreted as a direct temporal trend because Malé, MCOH, and MCOG represent different receptor environments. Malé is influenced by both local urban emissions and long-range transport; MCOH in the northern Maldives is particularly well positioned to intercept South Asian continental outflow, whereas MCOG lies approximately 800 km south of MCOH near the equator and is exposed to a stronger contrast between Northern Hemisphere continental influence and Southern Hemisphere marine air. In the year-round 2013 study, the annual mean $PM_{2.5}$ was 19 $\mu g\,m^{-3}$ at Malé and 13 $\mu g\,m^{-3}$ at MCOH, with approximately 70 % of Malé $PM_{2.5}$ attributable to long-range transport. During the dry season, MCOH $PM_{2.5}$, EC and OC were 19.5, 0.49 and 1.31 $\mu g\,m^{-3}$, respectively, compared with 21.2, 0.76 and 1.88 $\mu g\,m^{-3}$ at Malé, illustrating both the strong regional South Asian influence and the additional contribution from local emissions in the capital (Budhavant et al., 2015).

Subsequent observations at MCOH further established the strong seasonal contrast of this northern Indian Ocean receptor. During the winter of 2014–2015, mean $PM_{2.5}$, EC and OC were approximately 18.1, 0.59 and 1.22 $\mu g\,m^{-3}$, respectively, with substantially enhanced fine-mode anthropogenic aerosol during South Asian outflow (Budhavant et al., 2018). In contrast, five summer monsoon seasons at MCOH showed much lower BC and OC concentrations of 0.2 ± 0.2 and

$0.3 \pm 0.3\,\mu g\,m^{-3}$, respectively, together with nss-SO_4^{2-} of $1.1 \pm 1.0\,\mu g\,m^{-3}$ and BC-MAC_{678} of $7.6 \pm 2.5\,m^2\,g^{-1}$ (Budhavant et al., 2023). The radiocarbon measurements from that study indicated a highly variable but predominantly fossil BC contribution of about 65 ± 15 % during the summer monsoon.

The available observations from MCOG itself are much more limited. During the winter SAPOEX campaign, Budhavant et al. (2024) reported mean BC and OC concentrations at MCOG of about 0.3 ± 0.3 and $0.7 \pm 0.5\,\mu g\,m^{-3}$, respectively, with BC-$MAC_{678}$ of $7.0 \pm 1.9\,m^2\,g^{-1}$; during the common synoptic period, BC-MAC_{678} was $6.4 \pm 1.7\,m^2\,g^{-1}$. The present year-round MCOG observations therefore extend these earlier short-duration equatorial measurements across both monsoon regimes and transition periods. Rather than indicating a simple long-term increase or decrease, the comparison shows that aerosol characteristics across the Maldives depend strongly on receptor location, season, transport history, and wet removal. The particular contribution of the present dataset is the year-round characterisation of these processes at the near-equatorial MCOG receptor.

4 Conclusions and broader implications

This study provides a year-round characterisation of $PM_{2.5}$ chemical composition, aerosol optical properties, meteorology, air-mass transport, and supporting dual-carbon isotope signatures at MCOG, a near-equatorial receptor in the southern Maldives. The observations show clear differences between the NEM and SWM, likely arising from the combined effects of changing air-mass origin and monsoon meteorology, particularly precipitation and wet scavenging.

During the NEM, continental influence from South and Southeast Asia coincided with higher $PM_{2.5}$, BC, OC, nss-SO_4^{2-}, and AOD, whereas the SWM was characterised by lower aerosol loading and stronger marine influence. $PM_{2.5}$ and AOD_{500} were approximately 41 % and 35 % lower, respectively, during the SWM. The transition periods generally showed intermediate characteristics. Because the aerosol samples represent 72 h integrations, these changes are interpreted at the monsoon-regime scale rather than as responses to individual events.

In contrast to the strong seasonal changes in aerosol abundance and composition, BC-MAC_{658} differed only modestly between the NEM ($8.8 \pm 2.9\,m^2\,g^{-1}$) and SWM ($10.2 \pm 3.2\,m^2\,g^{-1}$), and the difference was not statistically significant. The present observations therefore do not demonstrate enhanced BC absorption caused by atmospheric ageing; rather, they indicate that BC mass-normalized absorption remains comparatively stable across the contrasting monsoon regimes.

The five dual-carbon isotope measurements show substantial sample-to-sample source variability within both monsoon periods and are therefore interpreted as complementary evidence rather than quantitative seasonal source apportionment.

Comparison with earlier observations from Malé, MCOH, and the Indian Ocean provides regional context but should not be interpreted as a direct temporal trend because the sites represent different receptor environments. The present dataset extends previous short-period observations at MCOG by providing year-round coverage of both monsoon regimes and their transition periods. Its near-equatorial location therefore provides a complementary constraint on aerosol transport, wet removal, composition, and optical properties for regional chemical-transport and Earth system models.

Data availability. The datasets generated and analysed in this study are provided as an Excel file in the Supplement accompanying this article. Additional data and information are available from the corresponding authors upon reasonable request.

Supplement. The supplement related to this article is available online at https://doi.org/10.5194/acp-26-16857-2026-supplement.

Author contributions. KBB and ÖG conceived and designed the study. AM, KBB, and JR conducted field sampling and collected aerosol samples at the Maldives Climate Observatory at Gan (MCOG). KBB performed the chemical, satellite data, and statistical analyses. KBB, JR, SKS, and ÖG interpreted the data. KBB prepared all figures and tables and wrote the first draft of the manuscript. All authors contributed to the interpretation of the results, reviewed and revised the manuscript, and approved the final version for publication.

Competing interests. The contact author has declared that none of the authors has any competing interests.

Disclaimer. Publisher's note: Copernicus Publications remains neutral with regard to jurisdictional claims made in the text, published maps, institutional affiliations, or any other geographical representation in this paper. The authors bear the ultimate responsibility for providing appropriate place names. Views expressed in the text are those of the authors and do not necessarily reflect the views of the publisher.

Acknowledgements. We gratefully acknowledge Mohamed Nazmee for his invaluable support with field sampling and observatory operations. We also sincerely thank the Maldives Meteorological Service (MMS) and the Government of the Republic of Maldives for their continued support of the joint operation of the Maldives Climate Observatory at Gan (MCOG).

Financial support. This research has been supported by the Svenska Forskningsrådet Formas (grant no. 2020-01917) and the Vetenskapsrådet (grant nos. 2017-01601 and 2020-05384).

The publication of this article was funded by the Swedish Research Council, Forte, Formas, and Vinnova.

Review statement. This paper was edited by Tuukka Petäjä and reviewed by two anonymous referees.

References

Andersson, A., Deng, J., Du, K., Zheng, M., Yan, C., Sköld, M., and Gustafsson, Ö.: Regionally varying combustion sources of the January 2013 severe haze events over eastern China, Environ. Sci. Technol., 49, 2038–2043, https://doi.org/10.1021/es503855e, 2015.

Bond, T. C., Doherty, S. J., Fahey, D. W., Forster, P. M., Berntsen, T., DeAngelo, B. J., Flanner, M. G., Ghan, S., Kärcher, B., Koch, D., Kinne, S., Kondo, Y., Quinn, P. K., Sarofim, M. C., Schultz, M. G., Schulz, M., Venkataraman, C., Zhang, H., Zhang, S., Bellouin, N., Guttikunda, S. K., Hopke, P. K., Jacobson, M. Z., Kaiser, J. W., Klimont, Z., Lohmann, U., Schwarz, J. P., Shindell, D., Storelvmo, T., Warren, S. G., and Zender, C. S.: Bounding the role of black carbon in the climate system: A scientific assessment, J. Geophys. Res.-Atmos., 118, 5380–5552, https://doi.org/10.1002/jgrd.50171, 2013.

Bosch, C., Andersson, A., Kirillova, E. N., Budhavant, K., Tiwari, S., Praveen, P. S., Russell, L. M., Beres, N. D., Ramanathan, V., and Gustafsson, Ö.: Source-diagnostic dual-isotope composition and optical properties of water-soluble black and elemental carbon in the South Asian outflow intercepted over the Indian Ocean, J. Geophys. Res.-Atmos., 119, 11743–11759, https://doi.org/10.1002/2014JD022127, 2014.

Budhavant, K., Andersson, A., Bosch, C., Kruså, M., Kirillova, E. N., Sheesley, R. J., Safai, P. D., Rao, P. S. P., and Gustafsson, Ö.: Radiocarbon-based source apportionment of elemental carbon aerosols at two South Asian receptor observatories over a full annual cycle, Environ. Res. Lett., 10, 064004, https://doi.org/10.1088/1748-9326/10/6/064004, 2015.

Budhavant, K., Bikkina, S., Andersson, A., Asmi, E., Kesti, J., Zahid, H., Satheesh, S. K., and Gustafsson, Ö.: Anthropogenic fine aerosols dominate the wintertime regime over the northern Indian Ocean, Tellus B, 70, 1464871, https://doi.org/10.1080/16000889.2018.1464871, 2018.

Budhavant, K., Andersson, A., Holmstrand, H., Bikkina, P., Bikkina, S., Satheesh, S. K., and Gustafsson, Ö.: Enhanced light absorption of black carbon in rainwater compared with aerosols over the northern Indian Ocean, J. Geophys. Res.-Atmos., 125, e2019JD031246, https://doi.org/10.1029/2019JD031246, 2020.

Budhavant, K., Andersson, A., Holmstrand, H., Satheesh, S. K., and Gustafsson, Ö.: Black carbon aerosols over the Indian Ocean have unique source fingerprints and optical characteristics during the monsoon season, Proc. Natl. Acad. Sci. USA, 120, e2210005120, https://doi.org/10.1073/pnas.2210005120, 2023.

Budhavant, K., Manoj, M. R., Nair, H. R. C. R., Gaita, S. M., Holmstrand, H., Salam, A., Muslim, A., Satheesh, S. K., and Gustafsson, Ö.: Changing optical properties of black carbon and brown carbon aerosols during long-range transport from the Indo-Gangetic Plain to the equatorial Indian Ocean, Atmos. Chem. Phys., 24, 11911–11925, https://doi.org/10.5194/acp-24-11911-2024, 2024.

Chen, B., Andersson, A., Lee, M., Kirillova, E. N., Xiao, Q., Kruså, M., Shi, M., Hu, K., Lu, Z., Streets, D. G., Du, K., and Gustafsson, Ö.: Source forensics of black carbon aerosols from China, Environ. Sci. Technol., 47, 9102–9108, https://doi.org/10.1021/es401599r, 2013.

Clarke, S., Holmstrand, H., Budhavant, K., Remani, M., Haslett, S., Rodiouchkina, K., Kooijman, E., and Gustafsson, Ö.: Isotopic apportionment of sulfate aerosols between natural and anthropogenic sources in the outflow of South Asia, Atmos. Chem. Phys., 26, 5333–5343, https://doi.org/10.5194/acp-26-5333-2026, 2026.

Corrigan, C. E., Ramanathan, V., and Schauer, J. J.: Impact of monsoon transition on the physical and optical properties of aerosols, J. Geophys. Res.-Atmos., 111, D18208, https://doi.org/10.1029/2005JD006370, 2006.

Dasari, S., Andersson, A., Stohl, A., Evangeliou, N., Bikkina, S., Holmstrand, H., Budhavant, K., Salam, A., and Gustafsson, Ö.: Source quantification of South Asian black carbon aerosols with isotopes and modelling, Environ. Sci. Technol., 54, 11771–11779, https://doi.org/10.1021/acs.est.0c02193, 2020.

Draxler, R. R. and Hess, G. D.: An overview of the HYSPLIT_4 modelling system for trajectories, dispersion, and deposition, Aust. Meteorol. Mag., 47, 295–308, 1998.

Giles, D. M., Sinyuk, A., Sorokin, M. G., Schafer, J. S., Smirnov, A., Slutsker, I., Eck, T. F., Holben, B. N., Lewis, J. R., Campbell, J. R., Welton, E. J., Korkin, S. V., and Lyapustin, A. I.: Advancements in the Aerosol Robotic Network (AERONET) Version 3 database – automated near-real-time quality control algorithm with improved cloud screening for Sun photometer aerosol optical depth (AOD) measurements, Atmos. Meas. Tech., 12, 169–209, https://doi.org/10.5194/amt-12-169-2019, 2019.

Gustafsson, Ö., Kruså, M., Zencak, Z., Sheesley, R. J., Granat, L., Engström, E., Praveen, P. S., Leck, C., and Rodhe, H.: Brown clouds over South Asia: Biomass or fossil fuel combustion?, Science, 323, 495–498, https://doi.org/10.1126/science.1164857, 2009.

Gustafsson, Ö., Budhavant, K., Chimurkar, N., Clarke, S., Dreyfus, G., Gong, X., Klimont, Z., Klingmüller, K., Kim, S.-W., Lelieveld, J., Myhre, G., Nair, H. R. C. R., Peng, J., Ramanathan, V., Rana, A., Manoj, M. R., Satheesh, S. K., Venkataraman, C., and Zhang, Q.: Atmospheric black carbon in the climate system, Nat. Rev. Earth Environ., https://doi.org/10.1038/s43017-026-00773-3, 2026.

Holben, B. N., Eck, T. F., Slutsker, I., Tanré, D., Buis, J. P., Setzer, A., Vermote, E., Reagan, J. A., Kaufman, Y. J., Nakajima, T., Lavenu, F., Jankowiak, I., and Smirnov, A.: AERONET – A federated instrument network and data archive for aerosol characterization, Remote Sens. Environ., 66, 1–16, https://doi.org/10.1016/S0034-4257(98)00031-5, 1998.

IPCC: Climate Change 2021: The Physical Science Basis, Contribution of Working Group I to the Sixth Assessment Report of the Intergovernmental Panel on Climate Change, Cambridge

University Press, Cambridge, UK and New York, NY, USA, https://doi.org/10.1017/9781009157896, 2021.

Keene, W. C., Pszenny, A. A. P., Galloway, J. N., and Hawley, M. E.: Sea-salt corrections and interpretation of constituent ratios in marine precipitation, J. Geophys. Res.-Atmos., 91, 6647–6658, https://doi.org/10.1029/JD091iD06p06647, 1986.

Kirillova, E. N., Andersson, A., Sheesley, R. J., Kruså, M., Praveen, P. S., Budhavant, K., Safai, P. D., Rao, P. S. P., and Gustafsson, Ö.: ^{13}C- and ^{14}C-based study of sources and atmospheric processing of water-soluble organic carbon (WSOC) in South Asian aerosols, J. Geophys. Res.-Atmos., 118, 614–626, https://doi.org/10.1002/jgrd.50130, 2013.

Kirillova, E. N., Andersson, A., Tiwari, S., Srivastava, A. K., Bisht, D. S., and Gustafsson, Ö.: Water-soluble organic carbon aerosols during a full New Delhi winter: Isotope-based source apportionment and optical properties, J. Geophys. Res.-Atmos., 119, 3476–3485, https://doi.org/10.1002/2013JD020041, 2014.

Li, Z., Lau, W. K.-M., Ramanathan, V., Wu, G., Ding, Y., Manoj, M. G., Liu, J., Qian, Y., Li, J., Zhou, T., Fan, J., Rosenfeld, D., Ming, Y., Wang, Y., Huang, J., Wang, B., Xu, X., Lee, S.-S., Cribb, M., Zhang, F., Yang, X., Zhao, C., Takemura, T., Wang, K., Xia, X., Yin, Y., Zhang, H., Guo, J., Zhai, P. M., Sugimoto, N., Babu, S. S., and Brasseur, G. P.: Aerosol and monsoon climate interactions over Asia, Rev. Geophys., 54, 866–929, https://doi.org/10.1002/2015RG000500, 2016.

Liu, D., Whitehead, J., Alfarra, M. R., Reyes-Villegas, E., Spracklen, D. V., Reddington, C. L., Kong, S., Williams, P. I., Ting, Y.-C., Haslett, S., Taylor, J. W., Flynn, M. J., Morgan, W. T., McFiggans, G., Coe, H., and Allan, J. D.: Black-carbon absorption enhancement in the atmosphere determined by particle mixing state, Nat. Geosci., 10, 184–188, https://doi.org/10.1038/ngeo2901, 2017.

Nair, H. R. C. R., Budhavant, K., Manoj, M. R., Kirillova, E. N., Satheesh, S. K., and Gustafsson, Ö.: Roles of water-soluble aerosol coatings for the enhanced radiative absorption of black carbon over South Asia and the northern Indian Ocean, Sci. Total Environ., 926, 171721, https://doi.org/10.1016/j.scitotenv.2024.171721, 2024.

Novakov, T., Andreae, M. O., Gabriel, R., Kirchstetter, T. W., Mayol-Bracero, O. L., and Ramanathan, V.: Origin of carbonaceous aerosols over the tropical Indian Ocean: Biomass burning or fossil fuels?, Geophys. Res. Lett., 27, 4061–4064, https://doi.org/10.1029/2000GL011759, 2000.

Ram, K. and Sarin, M. M.: Absorption coefficient and site-specific mass absorption efficiency of elemental carbon in aerosols from urban, rural and high-altitude sites in India, Environ. Sci. Technol., 43, 8233–8239, https://doi.org/10.1021/es9011542, 2009.

Ramanathan, V., Crutzen, P. J., Lelieveld, J., Mitra, A. P., Althausen, D., Anderson, J., Andreae, M. O., Cantrell, W., Cass, G. R., Chung, C. E., Clarke, A. D., Coakley, J. A., Dulac, F., Heintzenberg, J., Heymsfield, A. J., Holben, B., Howell, S., Hudson, J., Jayaraman, A., Kiehl, J. T., Krishnamurti, T. N., Lubin, D., McFarquhar, G., Novakov, T., Ogren, J. A., Podgorny, I., Prather, K., Priestley, K., Prospero, J. M., Quinn, P. K., Rajeev, K., Rasch, P., Rupert, S., Sadourny, R., Satheesh, S. K., Sheridan, P., Valero, F. P. J., and Xu, Y.: Indian Ocean Experiment: An integrated analysis of the climate forcing and effects of the great Indo-Asian haze, J. Geophys. Res.-Atmos., 106, 28371–28398, https://doi.org/10.1029/2001JD900133, 2001.

Safai, P. D., Budhavant, K. B., Rao, P. S. P., Ali, K., and Sinha, A.: Source characterization for aerosol constituents and changing roles of calcium and ammonium aerosols in the neutralization of aerosol acidity at a semi-urban site in SW India, Atmos. Res., 98, 78–88, https://doi.org/10.1016/j.atmosres.2010.05.011, 2010.

Sheesley, R. J., Kirillova, E. N., Andersson, A., Kruså, M., Praveen, P. S., Budhavant, K., Safai, P. D., Rao, P. S. P., and Gustafsson, Ö.: Year-round radiocarbon-based source apportionment of carbonaceous aerosols at two background sites in South Asia, J. Geophys. Res.-Atmos., 117, D10202, https://doi.org/10.1029/2011JD017161, 2012.

Stein, A. F., Draxler, R. R., Rolph, G. D., Stunder, B. J. B., Cohen, M. D., and Ngan, F.: NOAA's HYSPLIT atmospheric transport and dispersion modeling system, B. Am. Meteorol. Soc., 96, 2059–2077, https://doi.org/10.1175/BAMS-D-14-00110.1, 2015.

Stone, E. A., Lough, G. C., Schauer, J. J., Praveen, P. S., Corrigan, C. E., and Ramanathan, V.: Understanding the origin of black carbon in the atmospheric brown cloud over the Indian Ocean, J. Geophys. Res.-Atmos., 112, D22S23, https://doi.org/10.1029/2006JD008118, 2007.

Turpin, B. J. and Lim, H.-J.: Species contributions to $PM_{2.5}$ mass concentrations: Revisiting common assumptions for estimating organic mass, Aerosol Sci. Tech., 35, 602–610, https://doi.org/10.1080/02786820120648, 2001.

Weingartner, E., Saathoff, H., Schnaiter, M., Streit, N., Bitnar, B., and Baltensperger, U.: Absorption of light by soot particles: Determination of the absorption coefficient using Aethalometers, J. Aerosol. Sci., 34, 1445–1463, https://doi.org/10.1016/S0021-8502(03)00359-8, 2003.

Zencak, Z., Elmquist, M., and Gustafsson, Ö.: Quantification and radiocarbon source apportionment of black carbon in atmospheric aerosols using the CTO-375 method, Atmos. Environ., 41, 7895–7906, https://doi.org/10.1016/j.atmosenv.2007.06.006, 2007.